View metadata, citation and similar papers at core.ac.uk

brought to you by CORE

provided by Elsevier - Publisher Connector

Journal of Molecular and Cellular Cardiology 74 (2014) 220–230

Contents lists available at ScienceDirect

Journal of Molecular and Cellular Cardiology

journal homepage: www.elsevier.com/locate/yjmcc

Original article

Ranolazine inhibition of hERG potassium channels: Drug–pore interactions and reduced potency against inactivation mutants

Chunyun Du [a,1], Yihong Zhang [a,1], Aziza El Harchi [a], Christopher E. Dempsey [b], Jules C. Hancox [a,*]

[a] School of Physiology and Pharmacology and Cardiovascular Research Laboratories, Medical Sciences Building, University of Bristol, BS8 1TD, United Kingdom
[b] School of Biochemistry, Medical Sciences Building, University of Bristol, BS8 1TD, United Kingdom

ARTICLE INFO

Article history:
Received 17 April 2014
Received in revised form 14 May 2014
Accepted 19 May 2014
Available online 27 May 2014

Keywords:
Antiarrhythmic
Docking
hERG
Lidocaine
QT interval
Ranolazine

ABSTRACT

The antianginal drug ranolazine, which combines inhibitory actions on rapid and sustained sodium currents with inhibition of the hERG/I_{Kr} potassium channel, shows promise as an antiarrhythmic agent. This study investigated the structural basis of hERG block by ranolazine, with lidocaine used as a low potency, structurally similar comparator. Recordings of hERG current (I_{hERG}) were made from cell lines expressing wild-type (WT) or mutant hERG channels. Docking simulations were performed using homology models built on MthK and KvAP templates. In conventional voltage clamp, ranolazine inhibited I_{hERG} with an IC_{50} of 8.03 μM; peak I_{hERG} during ventricular action potential clamp was inhibited ~62% at 10 μM. The IC_{50} values for ranolazine inhibition of the S620T inactivation deficient and N588K attenuated inactivation mutants were respectively ~73-fold and ~15-fold that for WT I_{hERG}. Mutations near the bottom of the selectivity filter (V625A, S624A, T623A) exhibited IC_{50}s between ~8 and 19-fold that for WT I_{hERG}, whilst the Y652A and F656A S6 mutations had IC_{50}s ~22-fold and 53-fold WT controls. Low potency lidocaine was comparatively insensitive to both pore helix and S6 mutations, but was sensitive to direction of K^+ flux and particularly to loss of inactivation, with an IC_{50} for S620T-hERG ~49-fold that for WT I_{hERG}. Docking simulations indicated that the larger size of ranolazine gives it potential for a greater range of interactions with hERG pore side chains compared to lidocaine, in particular enabling interaction of its two aromatic groups with side chains of both Y652 and F656. The N588K mutation is responsible for the SQT1 variant of short QT syndrome and our data suggest that ranolazine is unlikely to be effective against I_{Kr}/hERG in SQT1 patients.

© 2014 The Authors. Published by Elsevier Ltd. This is an open access article under the CC BY-NC-ND license (http://creativecommons.org/licenses/by-nc-nd/3.0/).

1. Introduction

Class III antiarrhythmic agents prolong refractoriness and can be effective in treating atrial and ventricular re-entrant arrhythmias [1,2]. A number of 'pure' Class III compounds, including D-sotalol and dofetilide exert their effects through inhibition of the rapid delayed rectifier K^+ current, I_{Kr} and its recombinant equivalent hERG [3,4]. I_{Kr}/hERG blockade additionally contributes to the actions of the Class Ia antiarrhythmics quinidine and disopyramide and has also been reported for Class Ic drugs such as propafenone and flecainide (e.g. [5–8]). By contrast, the Class Ib antiarrhythmic agents mexiletine and lidocaine have comparatively low affinity for I_{Kr}/hERG channels [9–11]. Deleterious as well as beneficial effects of Class Ia and III drugs are associated with their I_{Kr}/hERG blocking propensity, as they carry some risk of acquired long QT syndrome and associated *Torsades de Pointes* (*TdP*) arrhythmia [12,13].

The antianginal agent ranolazine is receiving increasing interest as a potential antiarrhythmic agent [14,15]. In a pre-clinical experimental setting ranolazine can produce modest prolongation of action potential duration (APD; without reverse-rate dependence), without augmenting transmural dispersion of repolarization and it can suppress early afterdepolarizations in Purkinje fibres and ventricular 'M' cells; thus ranolazine appears to be without the potential to produce *TdP* of pure Class III drugs (reviewed in [16, 17]). Patients with angina receiving ranolazine exhibit concentration-dependent QT interval prolongation that is only modest at high doses (QT_c increase of <10 ms with 1000 mg twice daily; [18]). In humans, continuous ECG monitoring of 6351 patients over 7 days following admission for acute coronary syndrome (MERLIN-TIMI 36) showed that fewer patients on ranolazine had episodes of ventricular or supraventricular tachycardia, with a trend also towards a lower incidence of new onset atrial fibrillation (AF) [19]. A small-scale study of patients with new onset or paroxysmal atrial fibrillation (AF; most of whom had some structural heart disease) showed 72% (13/18 patients) conversion to sinus rhythm with high dose (2000 mg) ranolazine, suggesting that further evaluation of ranolazine for AF conversion is warranted [20]. A study of 25 patients with AF resistant to electrical cardioversion, found that 19 patients

* Corresponding author.
E-mail address: jules.hancox@bristol.ac.uk (J.C. Hancox).
[1] These authors contributed equally to this study.

http://dx.doi.org/10.1016/j.yjmcc.2014.05.013
0022-2828/© 2014 The Authors. Published by Elsevier Ltd. This is an open access article under the CC BY-NC-ND license (http://creativecommons.org/licenses/by-nc-nd/3.0/).

were successfully cardioverted within two attempts, following oral ranolazine administration [21].

Ranolazine exerts a use-dependent block of both rapid and sustained Na^+ currents (I_{Na} and $I_{Na,Late}$ respectively) [17,22,23] and due to differences between atrial and ventricular I_{Na}, the drug is considered to exhibit atrioselectivity of rapid I_{Na} blockade [24]. At clinically relevant concentrations, ranolazine also inhibits I_{Kr} and its recombinant equivalent 'hERG' [23,25,26]. Consequently, ranolazine combines clinically relevant actions against I_{Na} and I_{Kr} and this appears to lead to a more favourable frequency dependence of its effects on cardiac repolarization than seen with pure I_{Kr} blockade [27]. Indeed, ranolazine has a more favourable action on atrial effective refractory period than expected for pure I_{Kr} blockers such as dofetilide [28]. Ranolazine has been reported to produce I_{hERG} block that is rapid in its onset and reversibility and that depends on drug-access to the channel from the cell interior [26]. Additionally, whilst ranolazine does not impair trafficking of wild-type (WT) hERG channels to the cell membrane [26], a recent study suggests that it can promote trafficking of long QT syndrome (LQTS) mutant channels and thus ranolazine may have potential to act as a pharmacological chaperone for LQTS mutant hERG channels [29]. However, although there is evidence that ranolazine binds to hERG within the channel's inner cavity [23], the nature of the underlying drug–channel interactions is incompletely understood and the role of channel inactivation (which is critical for hERG inhibition by some, but not all, drugs [8,30]) in the drug's hERG blocking action has not been studied. Accordingly, the present investigation was undertaken to elucidate the nature and molecular determinants of the drug's inhibition of hERG, through a combination of electrophysiology and mutagenesis, together with drug docking to homology models of the hERG channel. As noted by others [31], ranolazine shares chemical structure with lidocaine (see Fig. S1 in the online supplement): both compounds exhibit a tertiary amine local anaesthetic (LA) structure containing hydrophobic (aromatic ring) and hydrophilic (tertiary amine) groups [31]. Lidocaine was therefore used as a low affinity [11], structurally similar comparator for experiments with hERG mutants and for docking.

2. Materials and methods

2.1. Maintenance of mammalian cell lines and cell transfection

HEK 293 cells stably expressing WT hERG (provided by Professor Craig January [32]) or the Y652A and F656A mutants [33] were maintained as described previously (e.g. [33,34]). For transient transfection, cells were maintained as previously described [35] and transfected with cDNA plasmids (T623A, S624A, V625A, N588K, S620T hERG) using either Lipofectamine 2000 or LTX (Invitrogen, Paisley, UK). Green Fluorescent Protein or CD8 was used as markers of successful transfection. Further details are available in the online supplementary information.

2.2. Electrophysiological recordings

Recordings were made at 37 ± 1 °C with a standard Tyrode's solution containing (in mM): 140 NaCl, 4 KCl, 2 $CaCl_2$, 1 $MgCl_2$, 10 Glucose, 5 HEPES (titrated to pH 7.4 with NaOH). For experiments with mutants T623A and F656A and their WT controls, the superfusate contained 94 mM KCl (with NaCl concentration correspondingly reduced) [34]. Patch-pipettes (Glass 8250, AM Systems Inc.) had a final resistance of 2–4 MΩ. The pipette dialysis solution contained (in mM): 130 KCl, 1 $MgCl_2$, 5 EGTA, 5 MgATP; pipette pH was buffered to pH 7.2 with 10 mM HEPES (titrated with KOH). Series resistance values typically lay between 3 and 7 MΩ and were compensated by ~60–80%. The data digitization rate was 10 kHz during all protocols and a bandwidth of 2 kHz was set on the amplifier. Further information, including specific equations used for data analysis, is available in the online supplementary information.

2.3. Ranolazine and lidocaine

Ranolazine di-HCl powder (Sequoia Research Products Ltd. UK) was dissolved in deionized water (Milli-Q, Millipore) to give a stock concentration of 10 mM. Lidocaine was dissolved in deionized water at a stock concentration of 10–20 mM. Both stock solutions were diluted with appropriate superfusion solutions to achieve series of concentration in the Results section. For higher final concentrations, lidocaine was dissolved directly in Tyrode's solution. All experimental superfusates during recording were delivered by a home-built rapid solution exchange device [36].

2.4. Molecular modelling

Docking of ranolazine and lidocaine to hERG was conducted using homology models of the hERG pore encompassing the pore helix, selectivity filter and S6 helices. As with previous studies we found that an open channel model built onto the crystal structure of the bacterial K^+ channel MthK (PDB: 1LNQ [37]) gave docking data broadly consistent with experimental mutagenesis data. This model is described elsewhere [34,38,39]. We have recently compared our MthK-based model with models based on putative C-type inactivated state structures of the KcsA bacterial channel and found that the MthK-based model accords more closely with experimental data on drug-binding for a range of structurally-diverse hERG blockers [39]. For other drugs that bind with moderate or weak affinity, binding modes obtained with a modified KvAP model ("Farid model") [40] were similar to those described for the MthK model [34]. Here docking was performed with both the MthK and Farid models using the Flexidock module of Sybylx2.0, which allows free sampling of protein side chain rotamers. Definition of the drug-binding pocket, selection of rotatable bonds, construction of starting configurations and choice of Genetic Algorithm parameters were performed as described previously [34,39]. Further information is available in the online supplementary information.

3. Results

3.1. Pharmacological sensitivity of WT I_{hERG}

The response of WT I_{hERG} to ranolazine was first determined using a ventricular action potential (AP) voltage command (AP clamp; Fig. 1Ai for representative traces and Fig. 1Aii for mean data). Application of 10 μM ranolazine produced I_{hERG} suppression that was rapid in both onset and reversibility (Fig. 1Aii). Peak I_{hERG} during the repolarizing phase of the AP was inhibited by 62.42 ± 2.03% (n = 6 cells). The rapid onset and washout of the effects of ranolazine are consistent with prior observations under conventional voltage clamp [26], in demonstrating that ranolazine inhibition both developed and washed out rapidly. We then used a conventional voltage step protocol, comprised of a 2-second depolarization to +20 mV followed by repolarization to −40 mV to elicit I_{hERG} tails. Tail current (I_{tail}) amplitude was measured relative to current elicited by a brief (50 ms) pre-pulse prior to the +20 mV test command [8,34,35,41]. Fig. 1B shows example records of I_{hERG} in control and in the presence of 10 μM ranolazine (with 58% blockade of the I_{hERG} tail in this example; (57.90 ± 1.29%, n = 6 cells; *t*-test, $p > 0.05$ compared to effects of this drug concentration under AP clamp)). The concentration–response relation for ranolazine inhibition of I_{hERG} elicited by this protocol is shown in Fig. 1D (filled squares), yielding an IC_{50} value of 8.03 ± 0.95 μM (h = 0.81 ± 0.07). Ranolazine thus produced I_{hERG} block at clinically relevant concentrations (2–6 μM [25]). For some drugs, reversal of the direction of K^+ ion flux can reduce I_{hERG} block, due to electrostatic repulsion or 'knock-off' (e.g.[30,34,42,43]). Therefore, we also sought concentration–response data for ranolazine for inward I_{hERG} currents at −120 mV, with a high (94 mM) extracellular K^+ concentration ($[K^+]_e$), using the protocol shown in Fig. 1C (lower panel). Representative current records

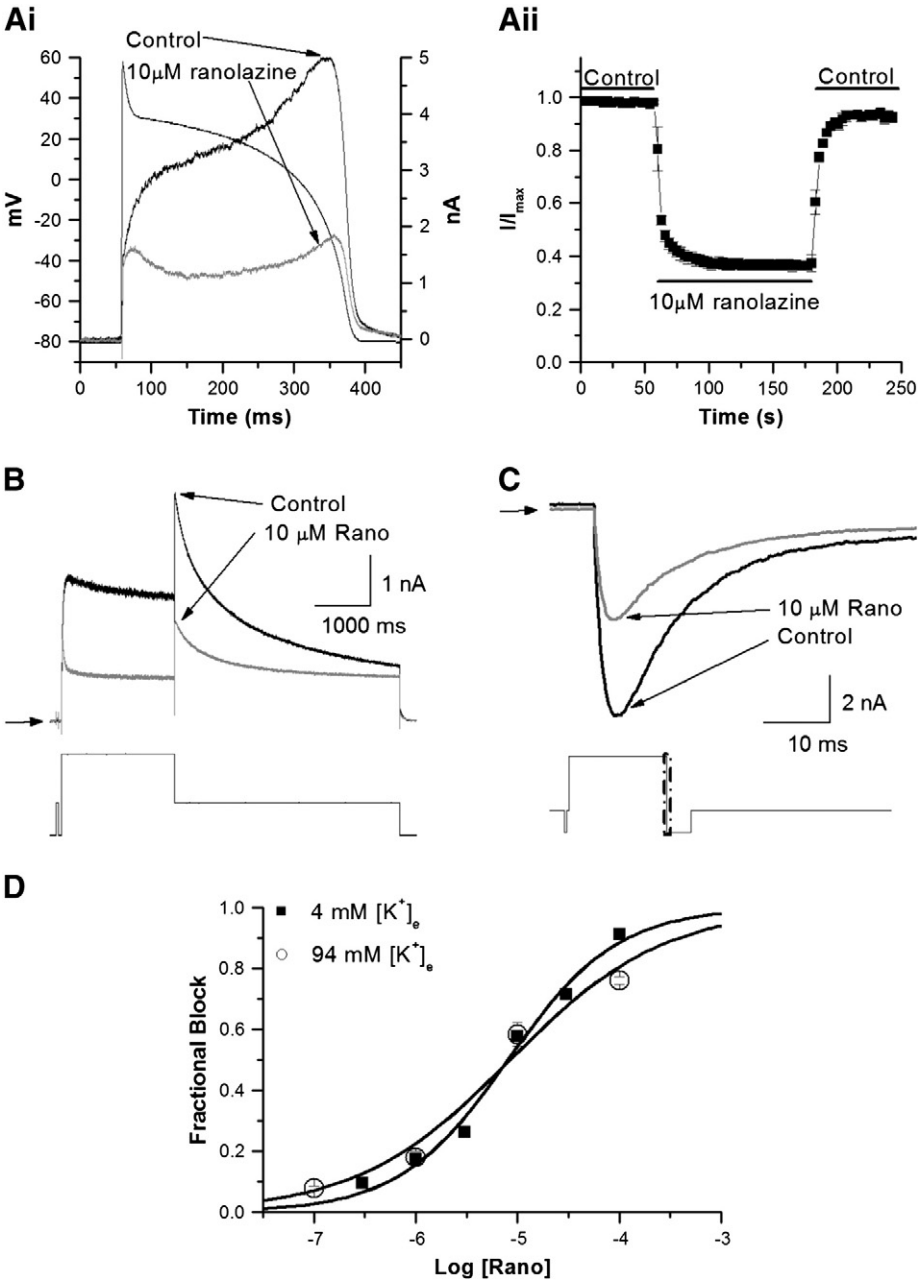

Fig. 1. Wild-type I_{hERG} block by ranolazine and lidocaine. Ai. Representative current traces in control (normal Tyrode's) solution and in 10 μM ranolazine, overlying the applied AP voltage command. Aii. Time-course of inhibition of peak I_{hERG} during the repolarization phase of the AP. Peak I_{hERG} in control was normalized to a value of 1 and then current magnitudes in ranolazine were expressed as a proportion of this (I/I_{max}; n = 6 cells). B. Upper panel shows representative I_{hERG} traces in the absence (black line) and presence (grey line) of 10 μM ranolazine in normal Tyrode's solution (4 mM $[K^+]_e$), elicited by the protocol shown in the lower panel. Horizontal arrows denote zero current. C. Upper panel shows inward I_{hERG} tail records in the absence (black line) and presence (grey line) of 10 μM ranolazine (~58% inhibition) in high K^+ Tyrode's solution (94 mM $[K^+]_e$). The current was evoked by the protocol shown in the lower panel and is shown on an expanded time-scale (denoted by the boxed area in the voltage protocol). D. Concentration–response relations for inhibition of I_{hERG} by ranolazine in normal K^+ (filled square) and high K^+ (open circle) Tyrode's solution. Data were fitted with a Hill-equation. Note that error bars for some points are small and are obscured by the symbols (n ≥ 5 cells per data-point). The data-points for 4 mM $[K^+]_e$ and 94 mM $[K^+]_e$ are closely overlain at 1 and 10 μM ranolazine.

are shown in Fig. 1C (upper panel), with concentration–response data plotted in Fig. 1D (open circles). The sensitivity of inward I_{hERG} to ranolazine in 94 mM $[K^+]_e$ (an IC_{50} value of 8.47 ± 2.63 μM; h = 0.58 ± 0.10) was similar to that for outward I_{hERG}. Parallel experiments were performed on lidocaine (see online supplemental Fig. S2 and Table S2). The IC_{50} for outward I_{hERG} tail inhibition by lidocaine in 4 mM $[K^+]_e$ was 141.77 ± 9.81 μM (h = 0.98 ± 0.07), with an IC_{50} for inward I_{hERG} in high $[K^+]_e$ increased to 735.32 ± 54.03 μM (h = 0.82 ± 0.05). Thus lidocaine differed from ranolazine both in its hERG blocking potency and sensitivity of inhibition to $[K^+]_e$ and to the direction of K^+ flux.

Further experiments were conducted under conventional voltage clamp in order to determine voltage dependence of WT I_{hERG} inhibition by ranolazine under our conditions (see supplemental Fig. S3 for details). Similar to a previous study [26], we observed ranolazine's inhibitory action to show a degree of voltage dependence and to be accompanied by a modest left-ward shift in voltage-dependent activation of I_{hERG} (by ~4 mV at 10 μM; see supplementary Fig. S3).

3.2. The effect of inactivation attenuation on I_{hERG} inhibition

Intact hERG channel inactivation is important to the development of I_{hERG} inhibition by some (typically, though not exclusively, high affinity) drugs [8,30,44], although some agents with sub-μM and μM IC_{50} values do not depend critically on inactivation gating for inhibition to occur

(e.g. [5,8,45]). To our knowledge, no previous study has investigated the extent to which channel inactivation is required for I_{hERG} inhibition by ranolazine. S620T hERG channels lack inactivation and have been suggested to be useful for determination of true drug affinity for the open/activated channel [30]. Fig. 2A shows the effects of S620T on I_{hERG} block by ranolazine (Fig. 2Ai (representative traces) and Aii (concentration–response relations)). The drug's inhibitory potency was markedly reduced for S620T hERG compared to the WT channel, with an IC_{50} value of 582.65 ± 23.36 μM (h = 0.89 ± 0.05), ~73-fold the WT IC_{50}. This mutation also had a marked effect on I_{hERG} block by lidocaine (see supplementary Fig. S4).

As ranolazine block of WT I_{hERG} occurs at clinically relevant concentrations, we further pursued the effect of inactivation attenuation by studying an additional, clinically relevant attenuated inactivation hERG mutant (N588K). Residue 588 lies in the S5-pore helix linker, which is distant from the hERG channel's inner cavity. In contrast to the S620T mutation [30,44], the N588K mutation does not eliminate I_{hERG} inactivation completely, but results in positively shifted voltage-dependent inactivation of I_{hERG} by ~+60 to +90 mV [46,47]. This mutation is responsible for one form (SQT1) of the genetic short QT syndrome. It markedly attenuates the action of Class III agents such as sotalol, dofetilide and E-4031, but produces relatively small effects on inhibition by Class Ia drugs [30,48]. Fig. 2Bi shows representative N588K I_{hERG} traces in control and in 10 μM ranolazine. I_{hERG} block was attenuated compared to that of WT I_{hERG}, but not as extensively as for the S620T mutation. Fig. 2Bii shows the concentration–response relation for inhibition of N588K I_{hERG} superimposed on that for WT I_{hERG}. The derived IC_{50} value was 124.08 ± 7.39 μM (h = 0.81 ± 0.05) for N588K hERG, ~15-fold the corresponding value for WT I_{hERG}. The reduction in ranolazine potency with this mutation is significantly greater than that reported for Class Ia or Class Ic drugs that have been studied previously [8,41,49,50].

3.3. Molecular determinants of ranolazine and lidocaine binding

The majority of hERG channel blockers studied bind within the channel's inner cavity, interacting with one or both of two S6 aromatic residues (Y652, F656) [3]. There is some evidence that ranolazine

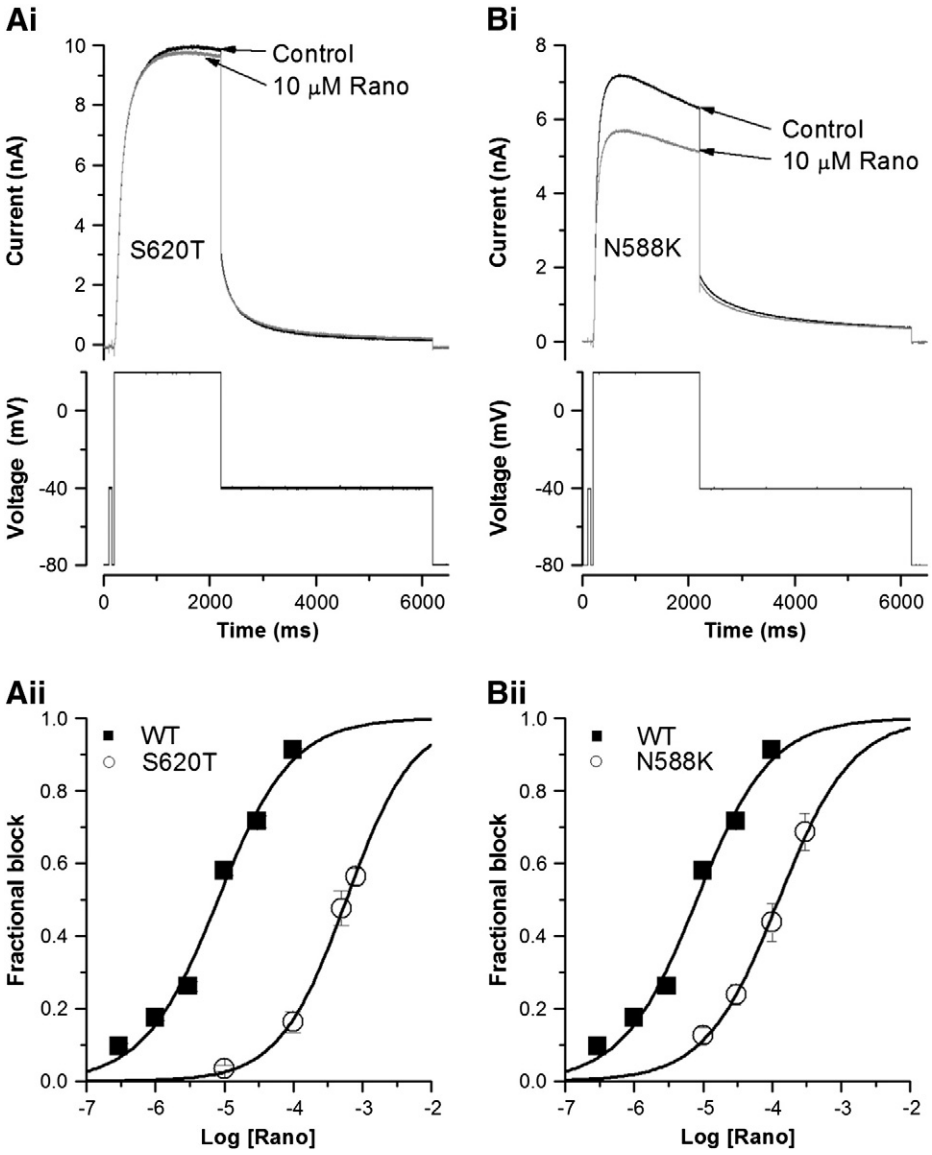

Fig. 2. Ranolazine block of S620T and N588K I_{hERG}. Ai, Bi. Representative S620T (Ai) and N588K (Bi) I_{hERG} traces in the absence (black line) and presence (grey line) of 10 μM ranolazine, elicited by the protocol shown in the lower panels. Aii, Bii. Concentration–response plots (mean ± SEM) for S620T I_{hERG} block by ranolazine (Aii) and N588K I_{hERG} block by ranolazine (Bii). In each case the relation for WT I_{hERG} during the same protocol is reproduced for comparison. Data were fitted with a Hill-equation. Error bars for some points are small and are obscured by the symbols. (n ≥ 5 cells per data-point.)

interacts with these aromatic residues [23]. We pursued this by measuring concentration–response data for Y652A and F656A hERG mutants with ranolazine and the structurally related lidocaine. Due to the known low expression and negatively shifted inactivation kinetics of F656A hERG [51], F656A I_{hERG} was evaluated by measuring inward tail current in high $[K^+]_e$ Tyrode (conditions comparable to those for WT I_{hERG} in Fig. 1C). Figs. 3 Ai and Aii show respectively the effects of ranolazine (10 μM) and lidocaine (300 μM) on F656A inward I_{hERG} tails compared with WT I_{hERG} controls. 10 μM ranolazine produced substantial inhibition of WT hERG tail current by 58.32 ± 3.87% (n = 6 cells). F656A hERG showed greatly attenuated I_{hERG} inhibition, with fractional block of only 6.62 ± 0.62% by 10 μM ranolazine (n = 5 cells). Fig. 3Bi shows concentration–response relations for WT and F656A I_{hERG}. The IC_{50} for F656A I_{hERG} was 452.67 ± 12.07 μM (*h* =

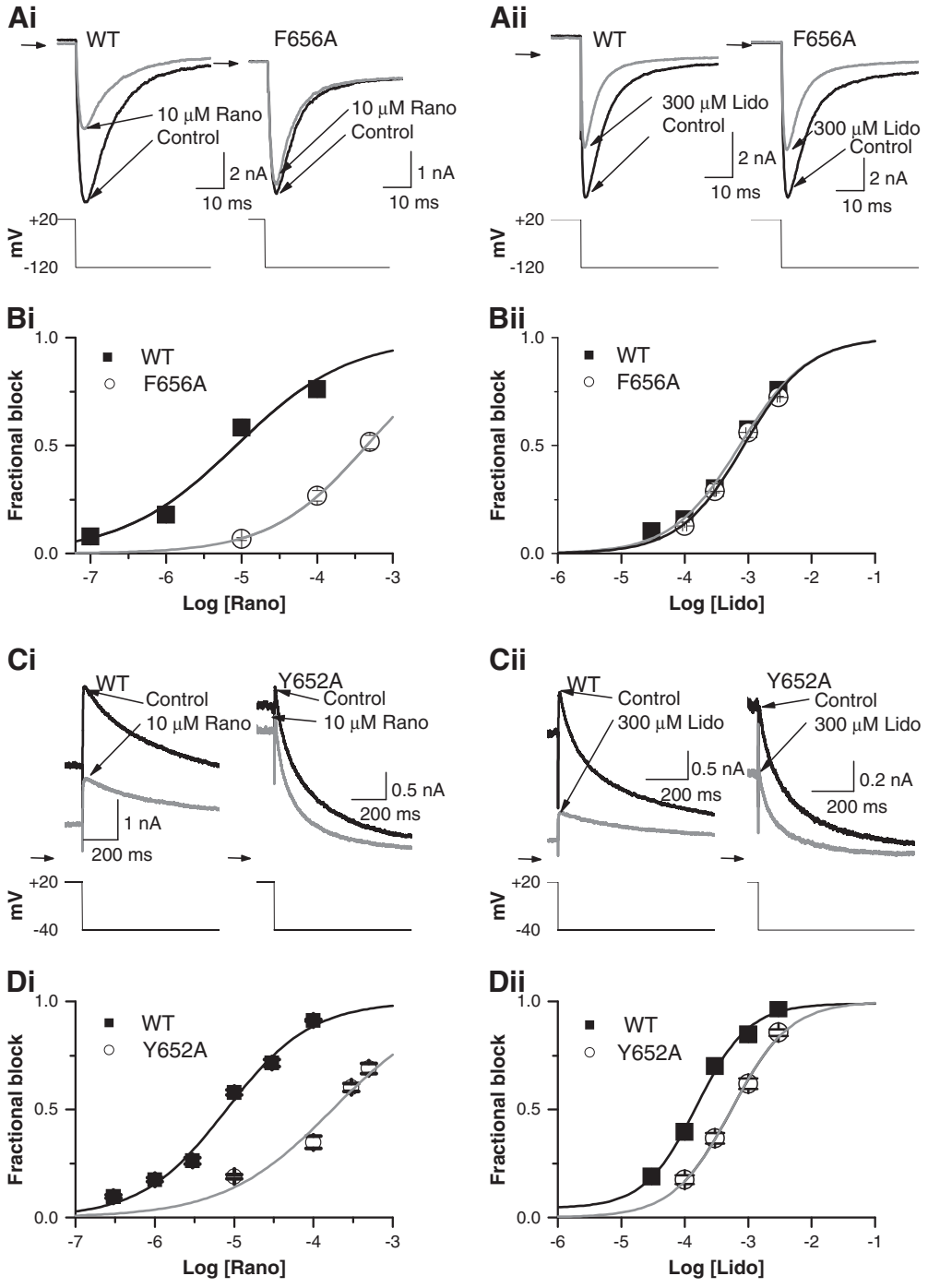

Fig. 3. Effect of S6 mutations on ranolazine and lidocaine block of I_{hERG}. A. Expanded representative I_{hERG} traces of WT hERG and F656A hERG in the absence (black line) and presence (grey line) of either 10 μM ranolazine (Ai) or 300 μM lidocaine (Aii). The current was evoked by the same protocol shown in Fig. 1C and was recorded in high K^+ Tyrode's solution (94 mM $[K^+]_e$). Horizontal arrows denote zero current. B. Concentration–response plots (mean ± SEM) for both WT (black line) and F656A (grey line) I_{hERG} block by ranolazine (Bi) and lidocaine (Bii). Data were fitted with a Hill-equation. Error bars for some points are small and are obscured by the symbols. (n ≥ 5 cells per data-point.) C. Expanded example I_{hERG} traces of WT hERG and Y652A hERG in the absence (black line) and presence (grey line) of either 10 μM ranolazine (Ci) or 300 μM lidocaine (Cii). The current was evoked by the same protocol shown in Fig. 1B and was recorded in normal Tyrode's solution (4 mM $[K^+]_e$). Horizontal arrows denote zero current. D. Concentration–response plots (mean ± SEM) for both WT (black line) and Y652A (grey line) I_{hERG} block by ranolazine (Di) and lidocaine (Dii). Data were fitted with a Hill-equation. Error bars for some points are small and are obscured by the symbols. (n ≥ 5 cells per data-point.)

0.68 ± 0.02), ~53-fold that of WT I_{hERG}. Fig. 3Aii shows that 300 μM lidocaine inhibited F656A inward I_{hERG} tails by 28.85 ± 1.80% (n = 8 cells) and WT I_{hERG} tails by 30.19 ± 2.09% (n = 6 cells). Fig. 3Bii shows concentration–response data for lidocaine against F656A I_{hERG}, which was closely superimposed over its WT control, with an IC_{50} value of 848.12 ± 65.54 μM (h = 0.85 ± 0.06), ~1.15-fold the value for WT. Thus, the F656 residue appeared to be a key binding determinant for ranolazine, but not for lidocaine.

The effect of Y652A on I_{hERG} inhibition by ranolazine and lidocaine is shown in Figs. 3C and D (with the standard voltage protocol used for WT I_{hERG}). Compared with the effect on WT I_{hERG} (Fig. 3Ci), inhibition of Y652A I_{hERG} by 10 μM ranolazine was significantly reduced (I_{tail} inhibition of ~19%). The concentration-dependence of mean fractional block is plotted in Fig. 3Di. The IC_{50} for inhibition of Y652A I_{hERG} by ranolazine was 173.62 ± 39.73 μM (h = 0.64 ± 0.14), ~22-fold the corresponding value for WT hERG. Figs. 3Cii and Dii show the effect of 300 μM lidocaine, with a reduction of the Y652A I_{tail} by ~36.64% compared to ~70.11% for the WT I_{tail}. The IC_{50} for inhibition of Y652A I_{hERG} by lidocaine was 554.33 ± 34.03 μM (h = 0.95 ± 0.06), ~3.8-fold the corresponding value for WT hERG. Thus, the Y652A mutation had a marked effect on ranolazine block of I_{hERG}, but only a modest effect on the action of lidocaine.

Amino acids located at the base of the pore helix (T623, S624 and V625) have been identified as important components of drug-binding sites for some [51–53] though not all [34,38] hERG blockers. To investigate the roles of these residues in ranolazine and lidocaine block the T623A, S624A and V652A mutations were studied. T623A I_{hERG} was studied using the same voltage protocol and conditions as used for

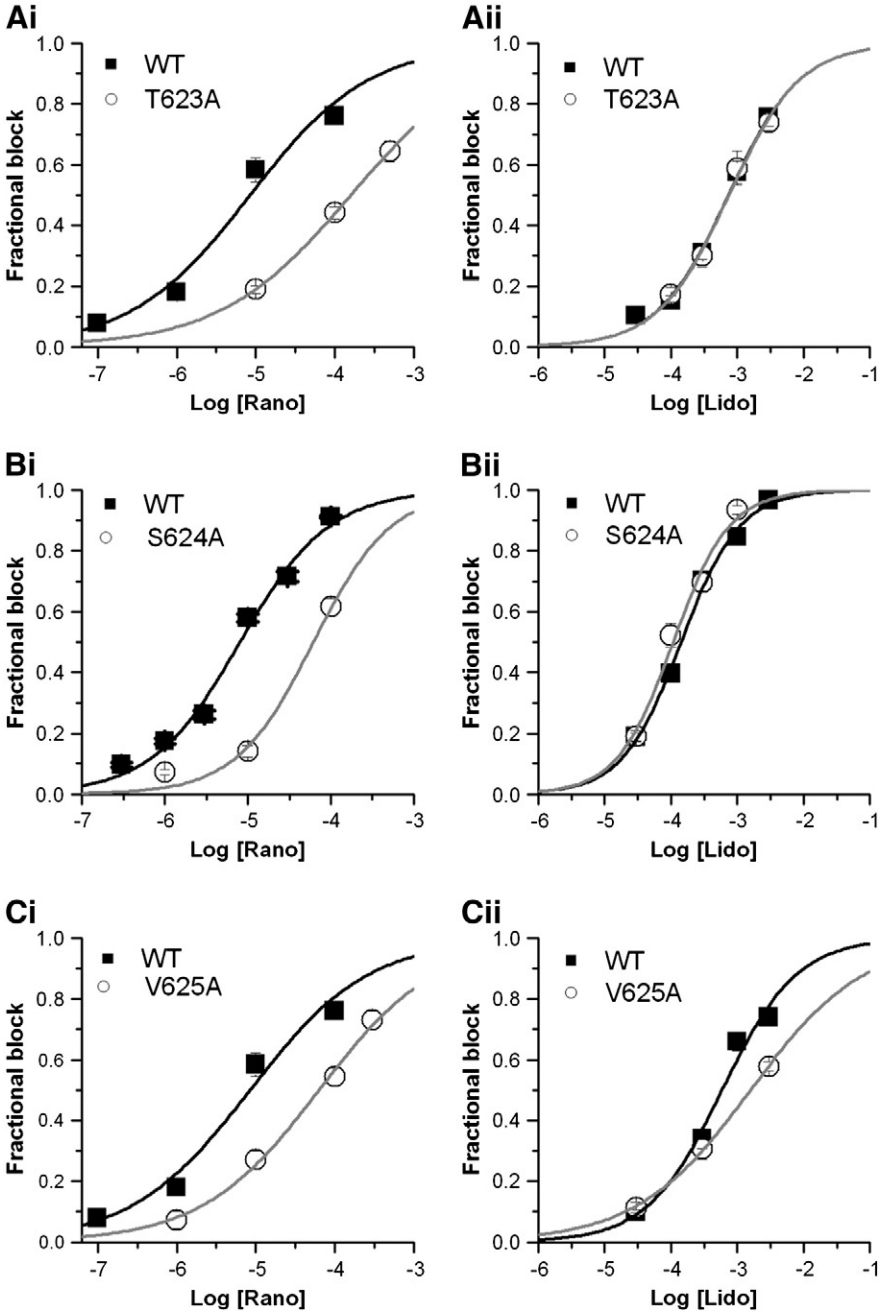

Fig. 4. Effect of pore helix mutations on ranolazine and lidocaine block of I_{hERG}. A. Fitted concentration–response relations for WT hERG (black line) and T623A hERG (grey line) inhibition by ranolazine (Ai) and lidocaine (Aii). Panels B, and C show equivalent data for T624A, and V625A, respectively. Error bars for some points are small and are obscured by the symbols. For all plots n ≥ 5 cells per data-point.

F656A I_{hERG}. Figs. 4Ai and Aii respectively show the concentration–response relations for ranolazine and lidocaine against WT and T623A I_{hERG}. The IC_{50} for T623A I_{hERG} block by ranolazine was 159.21 ± 2.42 μM ($h = 0.52 \pm 0.006$), ~19-fold its WT control (Fig. 4Ai), whilst that for lidocaine was 746.48 ± 70.40 μM ($h = 0.81 \pm 0.07$), 1.01-fold its WT control (Fig. 4Aii). The effect of S624A hERG on I_{hERG} block by ranolazine was investigated using the standard voltage protocol (shown in Fig. 1B). Figs. 4Bi and Bii show the concentration–response relations respectively for ranolazine and lidocaine for S624A I_{hERG}. The IC_{50} for S624A I_{hERG} block by ranolazine was 61.53 ± 12.93 μM ($h = 0.93 \pm 0.19$), ~8-fold that of WT I_{hERG} (Fig. 4Bi), whilst that for lidocaine was 107.59 ± 14.18 μM ($h = 1.03 \pm 0.14$), ~0.76-fold that of WT I_{hERG}. V625 is located within the K^+ signature sequence of hERG (SVGFG) and mutation to alanine reduces the selectivity of hERG channel for K^+ [51]. This mutant requires to be studied by measuring the inward hERG tail current at −120 mV. Fig. 4Ci shows concentration-response relations for WT and V625A I_{hERG} inhibition by ranolazine, with an IC_{50} of 63.14 ± 6.88 μM ($h = 0.58 \pm 0.04$), ~8-fold that of WT I_{hERG}. Fig. 4Cii shows similar data for lidocaine, which for V625A I_{hERG} had an IC_{50} of 1580 ± 75.48 μM ($h = 0.51 \pm 0.01$), 2.68-fold its WT control. Thus, each of the pore helix mutants had modest effects on ranolazine block of I_{hERG}, whilst for lidocaine T623A and S624A were essentially without effect and V625A had only a small effect.

The effects of all of the studied hERG mutants on the potency of inhibition of I_{hERG} by both ranolazine and lidocaine are summarized in supplementary Tables S1 and S2.

3.4. Molecular modelling of ranolazine and lidocaine action

Docking of lidocaine and ranolazine into the MthK and Farid models produced similar low energy score docked states. In both models the positively-charged tertiary amine common to both blockers was localized near the binding site for a K^+ ion observed in crystal structures of potassium channels (Fig. 5). K^+ ions are stabilised here by the focused

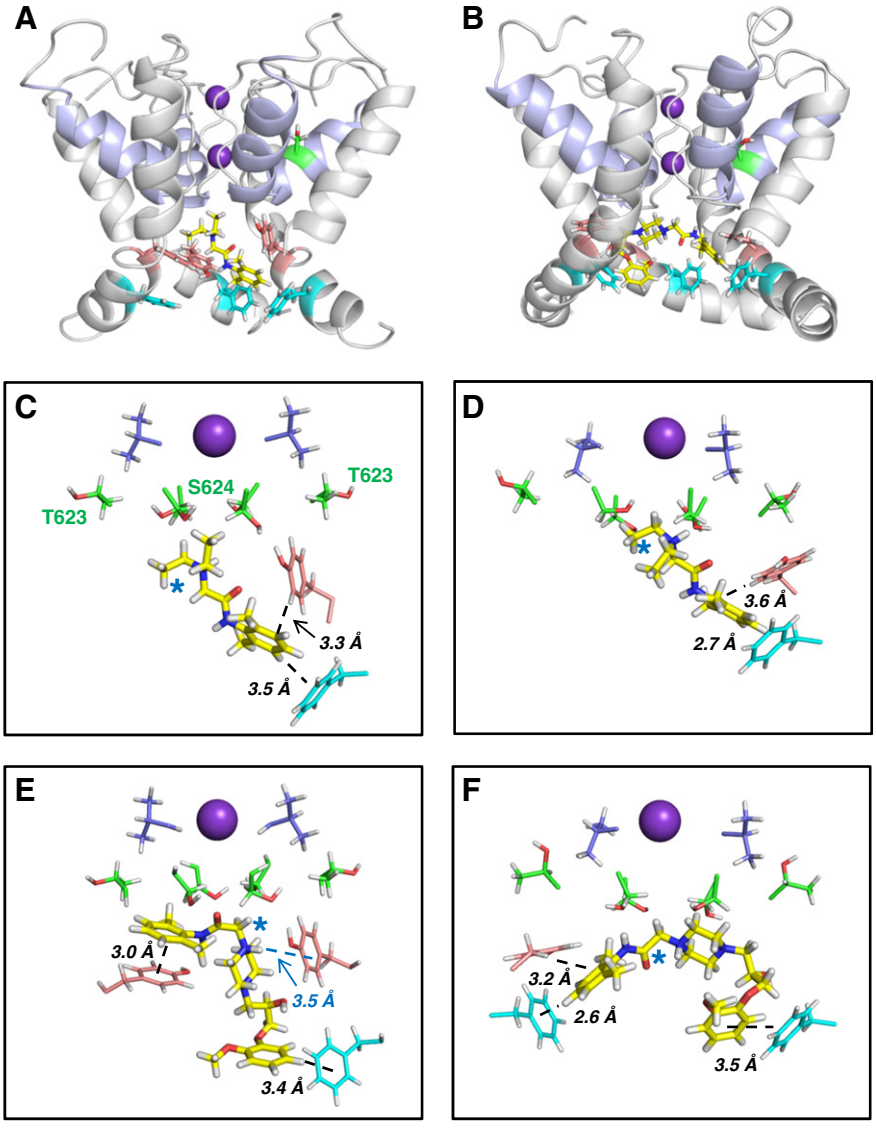

Fig. 5. Docking analysis of ranolazine and lidocaine action. A, B. Cut-away view of hERG pore homology models. (A) MthK-based model with a representative lidocaine binding pose; (B) the equivalent residues of the Farid model with a representative ranolazine binding pose. The pale blue ribbon defines the pore helices and K^+ ions in the S1 and S3 positions of the selectivity filter are purple spheres. Drug molecules are displayed as yellow sticks. Side chains of Y652 (salmon) and F656 (blue) are shown for three channel subunits. The side chain of one S620 residue (green) is shown for both models. C–F. Representative low energy score poses for lidocaine (C, D) and ranolazine (E, F) bound to the MthK-based model (C, E) or Farid model (D, F). The side chains of the aromatic side chains that make π–π or cation–π interactions with the drugs are shown in salmon (Y652) and light blue (F656). Side chains of T623 and S624 (green) and V625 (dark blue) are also shown as sticks. The K^+ ion in the S3 site of the selectivity filter is represented as a sphere. The blue star in each panel identifies the positively-charged tertiary alkyl amino groups of lidocaine and ranolazine.

electrostatic field arising from the C-terminal helix dipoles of the pore helices. In this configuration each blocker can make additional interactions with aromatic side chains of Y652 and F656. Neither drug made direct contact with V625 or S620 (Fig. 5), consistent with previous evidence that effects of S620T and V625A mutations on drug-binding result from indirect effects on hERG pore conformations (e.g. [54]). Although both drugs lie high in the pore cavity just below the selectivity filter, the orientations of the amide group differed, with the ranolazine amide lying horizontally in a position where it may hydrogen bond with the S624 side chain (Figs. 5B, E, F). The lidocaine amide was more vertically oriented and unable to hydrogen bond with the S624 OH group (Figs. 5A, C, D). These observations are consistent with the mutagenesis data for S624A (Figs. 4Bi, Bii). Similarly, lidocaine made no interactions with T623 (Figs. 5A, C, D) consistent with a lack of effect of T623A on lidocaine block (Fig. 4Aii). In some poses (e.g. Fig. 5E) ranolazine approached close to a T623 side chain; this may be relevant to the reduced block of T623A (Fig. 4Ai).

The structural basis for enhanced drug-binding to the hERG inactivated state has been attributed to the conformation of the S6 helix in which side chains, particularly Y652 and F656, are optimally positioned in the inactivated state to interact with drug molecules in the pore cavity [55]. The large suppression of ranolazine block in hERG S620T (Fig. 2Bi) is consistent with the multiple interactions of ranolazine moieties with Y652 and F656 side chains in WT hERG (Figs. 5E, F), and the attenuation of these interactions by non-optimal arrangements of aromatic side chains in S620T; this accounts for the observation that S620T produces a larger attenuation of block than either Y652A or F656A alone.

Lidocaine inhibition of I_{hERG} was substantially suppressed by the S620T mutation (supplemental Fig. S4). However, suppression of I_{hERG} block was negligible for F656A hERG (Fig. 3Bii) and only ~4-fold in Y652A (Fig. 3Dii), indicating that neither of these side chains is essential for block. Docking of lidocaine into hERG models carrying either the Y652A or F656A mutation showed that these observations may be understood in terms of a degeneracy in binding partners for the lidocaine aromatic group (supplemental Fig. S5); the lidocaine aromatic ring can make interactions with *either* a Y652 (in the case of F656A) *or* F656 (in Y652A) aromatic side chain. However if optimal configurations of both Y652 and F656 side chains are lost in S620T hERG, low affinity lidocaine block is considerably suppressed. By contrast, docking of ranolazine to models carrying either the Y652A or F656A mutation demonstrated that interactions with *both* Y652 and F656 aromatic side chains are required for optimal drug–pore interactions to occur (supplemental Fig. S6).

4. Discussion

4.1. Comparison with previous studies

The potency of I_{hERG} block by ranolazine reported here (IC_{50} of ~8 μM) is similar to that reported previously by Rajamani and colleagues (~12 μM) [26]. We found that ranolazine was nearly 18-fold more potent than lidocaine at inhibiting I_{hERG}, consistent with only a weak propensity of lidocaine to inhibit I_{hERG} [11]. Ranolazine has previously been suggested to compete with the methansulphonanilide E-4031 for a binding site on hERG [23], with some data supporting involvement of S6 aromatic residues in this action [23]. However, to our knowledge, no prior study has provided information on the role of inactivation gating in ranolazine's inhibitory action, nor a detailed analysis of structural determinants of inhibition. Nor, in contrast to its interactions with Na^+ channels [31,56], has any prior comparative analysis in respect of hERG block been conducted with lidocaine.

4.2. Role of inactivation in I_{hERG} block by ranolazine

The potency of ranolazine's inhibition of I_{hERG} reported here is similar to that of the Class Ia antiarrhythmic drug disopyramide (~7–11 μM [8,34]), but ranolazine differs markedly from disopyramide in two key respects: (i) disopyramide block is largely insensitive to mutations near the bottom of the selectivity filter (T623, S624, V625); (ii) disopyramide shows only a weak dependence of block on intact inactivation [8,34]. These characteristics are shared by other Class Ia/c drugs [8,38]. By contrast, the S620T-inactivation deficient channel showed markedly reduced sensitivity to ranolazine (and lidocaine). The location of the S620 residue on the pore helix and oriented towards the extracellular surface of the pore (Figs. 5A, B) excludes a direct interaction of this residue with drugs in the pore. Instead, the effect of S620T likely arises from the loss of configurations of side chains (especially Y652 and F656) upon inactivation gating that are favourable for drug interactions [55]. Indeed, titration of inactivation loss appears to produce a graded reduction in blocking potency of some drugs [8]. For ranolazine, the 72-fold reduction in the block of the S620T hERG mutant is similar to the sum of the individual reductions in block of hERG Y652A (22-fold) and F656A (53-fold), consistent with the expectation that ranolazine requires interactions with aromatic side chains of both residues to express full block. This is consistent with docking which shows simultaneous aromatic interactions with both Y652 and F656 residues (Fig. 5), and the loss of interactions in each of Y652A and F656A (Fig. S6). In contrast with the N588D (neutral ➔ negative charge substitution) long QT syndrome [56] mutation in the external S5-Pore linker, which results in a negative-shift in voltage-dependent I_{hERG} inactivation [57], the N588K (neutral ➔ positive charge substitution) short QT syndrome mutant produces a marked positive shift in voltage-dependent inactivation, but a change that is less extensive than for S620T [8,30]. Less extensive reduction in ranolazine block for N588K likely reflects the fact that inactivation is incompletely removed for N588K-hERG [8], so that interactions with aromatic residues are less extensively perturbed than for S620T. Moreover, in additional experiments performed on WT hERG, in which ranolazine was washed off gated hERG channels during sustained membrane depolarization (data not shown), the rate of current recovery was slowed at more depolarized voltages at which inactivation was promoted. This supports a role for inactivation gating in stabilizing ranolazine binding within the channel pore. In a previous investigation of the comparative pharmacology of the N588K short QT hERG mutant, there was a correlation between hERG blocking potency and sensitivity of block to attenuated inactivation [8]. However, despite a similar I_{hERG} blocking potency to disopyramide [8,34], ranolazine shows a much greater sensitivity to inactivation attenuation (~15-fold WT IC_{50} for N588K) than does disopyramide (~1.5 WT IC_{50} for N588K [8]). This argues against a fixed relationship between WT I_{hERG} blocking potency and dependence of blockade on inactivation. Our docking simulations (Fig. 5) indicated that ranolazine cannot interact directly with V625 whilst interacting with S6 aromatic residues. Consistent with suggestions for other drugs (e.g. [54]), the modest effect of V625A on ranolazine block of hERG is likely to arise from indirect effects of this mutation on the positioning of drug-binding residues.

4.3. Comparison between ranolazine and lidocaine

Lidocaine shares structural features with ranolazine but is a smaller molecule (see supplementary Fig. S1). Our findings indicate that the two drugs differ in their actions on hERG in the following respects: (i) inhibitory potency (ranolazine > lidocaine); (ii) sensitivity of inhibition to pore helix and S6 helix mutations; (iii) sensitivity of inhibition to potassium flux.

Mutagenesis and docking simulations demonstrate the potential for direct interactions between ranolazine and T623 and S624 residues, with hydrogen-bonding possible with S624 side chains. These interactions are absent for lidocaine. Ranolazine with two aromatic rings can make multiple interactions with Y652 and F656 side chains whereas the smaller lidocaine molecule makes fewer interactions (supplementary Fig. S7). Collectively, these factors can account for the greater inhibitory

potency of ranolazine than of lidocaine. As discussed above, the strong dependence of I_{hERG} inhibition by ranolazine on intact inactivation kinetics can be accounted for by optimal positioning of (S6) binding residues. For lidocaine, the effect of the S620T mutation (a 48-fold higher IC_{50} in potency) was much greater than that of either Y652A (3.84-fold WT IC_{50}) or F656A (1.15-fold WT IC_{50}) or their sum. Lidocaine possesses both an aromatic ring and a charged aliphatic amine group that can be anticipated to interact with aromatic side chains (through π–π and cation–π interactions respectively). Indeed, block of voltage gated Na^+ channels by local anaesthetics relies on Phe and Tyr residues (equivalent to F1670 and Y1767 in Nav1.5 isoform-1) in the S6 segment of domain 4, [58,59] with the Phe likely interacting directly with lidocaine through a cation–π interaction [60]. Ranolazine's inhibitory action on both peak and persistent Na_v 1.5 current is sensitive to mutation of F1760[20], indicating a common binding site for lidocaine and ranolazine on Na_v channels (although the underlying molecular interactions may differ [58]). Thus, it seems reasonable to propose that lidocaine is also likely to interact with S6 aromatic residues of hERG and our docking data (Figs. 5 and S5) support such a conclusion. Mutagenesis and docking data can be reconciled by degeneracy of lidocaine interactions with the two aromatic residues: the docking simulations suggest that the aromatic ring of lidocaine can interact with *either* F656 or Y652 residues. We attribute the marked reduction in lidocaine's I_{hERG} inhibitory action by the S620T inactivation mutant to the loss of favourable configurations of *both* Y652 and F656 in S620T, with the consequence that the aromatic group of lidocaine is unable to make any aromatic interactions within the pore cavity (Figs. 5 and S5).

Consistent with our interpretations for hERG (Figs. 5 and S5), modelling of lidocaine binding to the open state Na_v channel supports binding poses in which the positively-charged amino group is located below the selectivity filter where the pore helix negative dipole charges are focussed [60]. This binding mode makes lidocaine block susceptible to competing charge effects (in the case of Na_v as a result of charge repulsion between lidocaine and a Na^+ ion in its DEKA binding site in non-inactivated states [60]). This is manifest in hERG as a reduction of lidocaine block by competition from K^+ ions under conditions of inward ion flux (Figs. 1Cii and Dii). The docked poses for lidocaine (Figs. 5 and S5) suggest an explanation for the reduction in hERG block by inward K^+ flux, since binding interactions comprise only the tertiary amino group with the pore helix dipole charges and the aromatic ring with either a Y652 or F656 side chain. The electrostatic interaction constitutes a large proportion of the total contributions to binding so that competition with permeant ions for the K^+ binding site significantly reduces lidocaine affinity. The electrostatic component makes a much smaller contribution to binding for ranolazine which is relatively resistant to the effects of permeant ions.

4.4. Significance for clinical drug use and development

Recent human subject data indicate that plasma concentrations (C_{max}) of ranolazine of 741.5 ng/ml and 2328.7 ng/ml (~1.73 and ~4.05 μM) are attained after single oral doses of 500 mg and 1500 mg respectively [61]. These levels are in good agreement with a clinical plasma concentration range of 2–6 μM quoted by Rajamani and colleagues [25]. Thus, partial I_{hERG}/I_{Kr} inhibition can be expected to occur during clinical use of ranolazine. By contrast, plasma lidocaine levels during clinical use approximate ~7–15 μM [62,63] and, with an IC_{50} for I_{hERG} inhibition close to 142 μM, lidocaine is anticipated to produce little or no I_{hERG}/I_{Kr} inhibition during therapeutic use. Our results explain why ranolazine is able to inhibit $hERG/I_{Kr}$ at clinically relevant concentrations, whilst structurally similar lidocaine only produces significant inhibition at concentrations markedly exceeding the normal clinical range. Although ranolazine can exert weak actions on other ionic currents, the dominant ventricular ion channel effects of ranolazine at therapeutic concentrations are inhibition of $I_{Na,Late}$ and I_{Kr}, whilst comparatively atrioselective inhibition of rapid, peak I_{Na} [24] additionally contributes importantly to the atrial actions of the drug [64,65]. The I_{Kr} blocking effect of ranolazine has been proposed to be significant to the drug's action against AF [24,28,64]. The greater atrial than ventricular APD-prolonging effect of the drug may result from differences in AP configuration (and roles of $I_{Na,Late}$) in the two tissue types, whilst the drug's I_{Kr} blockade enhances inactivated state Na^+ channel block and therefore ranolazine's overall effectiveness [24,64].

The larger size of ranolazine gives it potential for a greater range of interactions with hERG pore side chains compared to lidocaine, and enables interaction of its two aromatic groups with side chains of both Y652 and F656. Our analysis indicates that low potency lidocaine block has low susceptibility to either of the Y652A and F656A mutations because either aromatic side chain can “compensate” for loss of the other. Given that combining Na^+ channel and I_{Kr} actions may hold promise for antiarrhythmic drug rate-dependency [27,66–68], the comparative information on ranolazine and lidocaine in this study in respect of hERG block may feasibly have utility for future design of agents combining I_{Na} and I_{Kr} inhibition, through modification(s) of the lidocaine template that is common to both drugs. Our data in respect of ranolazine are also of significance to pharmacological treatment of the hERG-linked (SQT1) variant of the genetic short QT syndrome. Patients with N588K-hERG-linked SQT1 are at risk of ventricular arrhythmia and sudden death and are usually treated an implantable cardioverter defibrillator, which itself carries a risk of inappropriate shocks [69]. This makes antiarrhythmic treatment an attractive adjunct approach. However, ranolazine inhibition of I_{hERG} at clinically relevant drug concentrations appears to require intact inactivation and, in particular, the reduction in ranolazine potency with the N588K hERG mutation seen here is significantly greater than that reported for Class Ia or Class Ic drugs that have been studied previously [8,41,49,50]. Consequently, ranolazine is unlikely to be a suitable alternative to Class Ia antiarrhythmic agents currently used for the pharmacological treatment of SQT1 [70].

Acknowledgments

JCH and CED thank the British Heart Foundation and Heart Research UK for funding. YHZ was funded by BHF PG/10/17 and PG/12/69. AEH was funded by BHF PG/09/34 and PG/10/36. CYD was funded by HRUK RG2541 and RG2594.

Appendix A. Supplementary data

Supplementary data to this article can be found online at http://dx.doi.org/10.1016/j.yjmcc.2014.05.013.

Conflict of interest statement

None.

References

[1] Nattel S. Class III drugs: amiodarone, bretylium, ibutilide and sotalol. In: Zipes DP, Jalife J, editors. Cardiac electrophysiology; from cell to bedside; 3rd ed. 1999. p. 921–32.
[2] Hondeghem LM, Snyders DJ. Class III antiarrhythmic agents have a lot of potential but a long way to go. Circulation 1990;81:686–90.
[3] Sanguinetti MC, Tristani-Firouzi M. hERG potassium channels and cardiac arrhythmia. Nature March 23 2006;440:463–9.
[4] Hancox JC, McPate MJ, El Harchi A, Zhang YH. The hERG potassium channel and hERG screening for drug-induced torsades de pointes. Pharmacol Ther 2008;119:118–32.
[5] Lees-Miller JP, Duan Y, Teng GQ, Duff HJ. Molecular determinant of high affinity dofetilide binding to HERG1 expressed in Xenopus oocytes: involvement of S6 sites. Mol Pharmacol 2000;57:367–74.
[6] Paul AA, Witchel HJ, Hancox JC. Inhibition of HERG potassium channel current by the Class 1a antiarrhythmic agent disopyramide. Biochem Biophys Res Commun 2001;280:1243–50.

[7] Arias C, Gonzalez T, Moreno I, Caballero R, Delpon E, Tamargo J, et al. Effects of propafenone and its main metabolite, 5-hydroxypropafenone, on HERG channels. Cardiovasc Res 2003;57(3):660–9.
[8] McPate MJ, Duncan RS, Hancox JC, Witchel HJ. Pharmacology of the short QT syndrome N588K-hERG K^+ channel mutation: differential impact on selected class I and class III antiarrhythmic drugs. Br J Pharmacol 2008;155:957–66.
[9] Wang DW, Kiyosue T, Sato T, Arita M. Comparison of the effects of Class-I antiarrhythmic drugs, cibenzoline, mexiletine and flecainide, on the delayed rectifier K current of guinea-pig ventricular myocytes. J Mol Cell Cardiol 1996;28:893–903.
[10] Mitcheson JS, Hancox JC. Modulation by mexiletine of action potentials, L-type Ca current and delayed rectifier K current recorded from isolated rabbit atrioventricular nodal myocytes. Pflugers Arch 1997;434:855–8.
[11] Paul AA, Witchel HJ, Hancox JC. Inhibition of heterologously expressed HERG potassium channels by flecainide and comparison with quinidine, propafenone and lignocaine. Br J Pharmacol 2002;136:717–29.
[12] Viskin S. Long QT, syndromes and torsade de pointes. Lancet 1999;354:1625–33.
[13] Yap YG, Camm AJ. Drug induced QT prolongation and torsades de pointes. Heart 2003;89:1363–72.
[14] Hancox JC, Doggrell SA. Perspective: does ranolazine have potential for the treatment of atrial fibrillation? Expert Opin Investig Drugs 2010;19:1465–74.
[15] Saklani P, Skanes A. Novel anti-arrhythmic medications in the treatment of atrial fibrillation. Curr Cardiol Rev 2012;8:302–9.
[16] Singh BN, Wadhani N. Antiarrhythmic and proarrhythmic properties of QT-prolonging antianginal drugs. J Cardiovasc Pharmacol Ther 2004;9:S85–97.
[17] Zaza A, Belardinelli L, Shryock JC. Pathophysiology and pharmacology of the cardiac "late sodium current.". Pharmacol Ther 2008;119:326–39.
[18] Chaitman BR. Efficacy and safety of a metabolic modulator drug in chronic stable angina: review of evidence from clinical trials. J Cardiovasc Pharmacol Ther 2004;9:S47–64.
[19] Scirica BM, Morrow DA, Hod H, Murphy SA, Belardinelli L, Hedgepath CM, et al. Effect of ranolazine, an antianginal agent with novel electrophysiological properties, on the incidence of arrhythmias in patients with non ST-segment elevation acute coronary syndrome: results from the Metabolic Efficiency With Ranolazine for Less Ischemia in Non ST-Elevation Acute Coronary Syndrome Thrombolysis in Myocardial Infarction 36 (MERLIN-TIMI 36) randomized controlled trial. Circulation 2007;116:1647–52.
[20] Murdock DK, Kersten M, Kaliebe J, Larrain G. The use of oral ranolazine to convert new or paroxysmal atrial fibrillation: a review of experience with implications for possible "pill in the pocket" approach to atrial fibrillation. Indian Pacing Electrophysiol J 2009;9:260–7.
[21] Murdock DK, Kaliebe J, Larrain G. The use of ranolazine to facilitate electrical cardioversion in cardioversion-resistant patients: a case series. Pacing Clin Electrophysiol 2012;35:302–7.
[22] Rajamani S, El-Bizri N, Shryock JC, Makielski JC, Belardinelli L. Use-dependent block of cardiac late Na^+ current by ranolazine. Heart Rhythm 2009;6:1625–31.
[23] Wu L, Rajamani S, Li H, January CT, Shryock JC, Belardinelli L. Reduction of repolarization reserve unmasks the proarrhythmic role of endogenous late Na^+ current in the heart. Am J Physiol Heart Circ Physiol 2009;297:H1048–57.
[24] Burashnikov A, Di Diego JM, Zygmunt AC, Belardinelli L, Antzelevitch C. Atrium-selective sodium channel block as a strategy for suppression of atrial fibrillation: differences in sodium channel inactivation between atria and ventricles and the role of ranolazine. Circulation 2007;116:1449–57.
[25] Antzelevitch C, Belardinelli L, Wu L, Fraser H, Zygmunt AC, Burashnikov A, et al. Electrophysiologic properties and antiarrhythmic actions of a novel antianginal agent. J Cardiovasc Pharmacol Ther 2004 September;9(Suppl. 1):S65–83.
[26] Rajamani S, Shryock JC, Belardinelli L. Rapid kinetic interactions of ranolazine with HERG K^+ current. J Cardiovasc Pharmacol 2008;51:581–9.
[27] Trenor B, Gomis-Tena J, Cardona K, Romero L, Rajamani S, Belardinelli L, et al. In silico assessment of drug safety in human heart applied to late sodium current blockers. Channels (Austin) 2013;7:249–62 [21].
[28] Kumar K, Nearing BD, Carvas M, Nascimento BC, Acar M, Belardinelli L, et al. Ranolazine exerts potent effects on atrial electrical properties and abbreviates atrial fibrillation duration in the intact porcine heart. J Cardiovasc Electrophysiol 2009;20:796–802.
[29] Smith JL, Reloj AR, Nataraj PS, Bartos DC, Schroder EA, Moss AJ, et al. Pharmacological correction of long QT-linked mutations in KCNH2 (hERG) increases the trafficking of Kv11.1 channels stored in the transitional endoplasmic reticulum. Am J Physiol Cell Physiol 2013;305:C919–30.
[30] Perrin MJ, Kuchel PW, Campbell TJ, Vandenberg JI. Drug binding to the inactivated state is necessary but not sufficient for high-affinity binding to human ether-à-go-go-related gene channels. Mol Pharmacol 2008;74:1443–52.
[31] Fredj S, Sampson KJ, Liu H, Kass RS. Molecular basis of ranolazine block of LQT-3 mutant sodium channels: evidence for site of action. Br J Pharmacol 2006;148:16–24.
[32] Zhou Z, Gong Q, Ye B, Fan Z, Makielski JC, Robertson GA, et al. Properties of HERG channels stably expressed in HEK 293 cells studied at physiological temperature. Biophys J 1998;74:230–41.
[33] Milnes JT, Crociani O, Arcangeli A, Hancox JC, Witchel HJ. Blockade of HERG potassium currents by fluvoxamine: incomplete attenuation by S6 mutations at F656 or Y652. Br J Pharmacol 2003;139:887–98.
[34] El Harchi A, Zhang YH, Hussein L, Dempsey CE, Hancox JC. Molecular determinants of hERG potassium channel inhibition by disopyramide. J Mol Cell Cardiol 2012;52:185–95.
[35] Zhang YH, Colenso CK, Sessions RB, Dempsey CE, Hancox JC. The hERG K^+ channel S4 domain L532P mutation: characterization at 37 °C. Biochim Biophys Acta 1808;2011:2477–87.
[36] Levi AJ, Hancox JC, Howarth FC, Croker J, Vinnicombe J. A method for making rapid changes of superfusate whilst maintaining temperature at 37 °C. Pflugers Arch 1996;432:930–7.
[37] Jiang Y, Lee A, Chen J, Cadene M, Chait BT, MacKinnon R. Crystal structure and mechanism of a calcium-gated potassium channel. Nature 2002;417:515–22.
[38] Witchel HJ, Dempsey CE, Sessions RB, Perry M, Milnes JT, Hancox JC, et al. The low-potency, voltage-dependent HERG channel blocker propafenone — molecular determinants and drug trapping. Mol Pharmacol 2004;66:1201–12.
[39] Dempsey CE, Wright D, Colenso CK, Sessions RB, Hancox JC. Assessing HERG pore models as templates for drug docking using published experimental constraints: the inactivated state in the context of drug block. J Chem Inf Model 2014;54:601–12.
[40] Farid R, Day T, Friesner RA, Pearlstein RA. New insights about HERG blockade obtained from protein modeling, potential energy mapping, and docking studies. Bioorg Med Chem 2006;14:3160–73.
[41] McPate MJ, Duncan RS, Witchel HJ, Hancox JC. Disopyramide is an effective inhibitor of mutant HERG K^+ channels involved in variant 1 short QT syndrome. J Mol Cell Cardiol 2006;41:563–6.
[42] Yang T, Roden DM. Extracellular potassium modulation of drug block of I_{Kr}. Implications for torsade de pointes and reverse use-dependence. Circulation 1996;93:407–11.
[43] Barrows B, Cheung K, Bialobrzeski T, Foster J, Schulze J, Miller A. Extracellular potassium dependency of block of HERG by quinidine and cisapride is primarily determined by the permeant ion and not by inactivation. Channels (Austin) 2009;3:239–48.
[44] Ficker E, Jarolimek W, Kiehn J, Baumann A, Brown AM. Molecular determinants of dofetilide block of HERG K channels. Circ Res 1998;82:386–95.
[45] Duncan RS, McPate MJ, Ridley JM, Gao Z, James AF, Leishman DJ, et al. Inhibition of the HERG potassium channel by the tricyclic antidepressant doxepin. Biochem Pharmacol 2007;74:425–37.
[46] Cordeiro JM, Brugada R, Wu YS, Hong K, Dumaine R. Modulation of I_{Kr} inactivation by mutation N588K in KCNH2: a link to arrhythmogenesis in short QT syndrome. Cardiovas Res 2005;67:498–509.
[47] McPate MJ, Duncan RS, Milnes JT, Witchel HJ, Hancox JC. The N588K-HERG K^+ channel mutation in the 'short QT syndrome': mechanism of gain-in-function determined at 37 °C. Biochem Biophys Res Commun 2005;334:441–9.
[48] Wolpert C, Schimpf R, Giustetto C, Antzelevitch C, Cordeiro J, Dumaine R, et al. Further insights into the effect of quinidine in short QT syndrome caused by a mutation in HERG. J Cardiovasc Electrophysiol 2005;16:54–8.
[49] Brugada R, Hong K, Dumaine R, Cordeiro J, Gaita F, Borgreffe M, et al. Sudden death associated with short-QT syndrome linked to mutations in HERG. Circulation 2004;109:30–5.
[50] Hong K, Bjeerregaard P, Gussak I, Brugada R. Short QT syndrome and atrial fibrillation caused by mutation in KCNH2. J Cardiovasc Electrophysiol 2005;16:394–6.
[51] Mitcheson JS, Chen J, Lin M, Culberson C, Sanguinetti MC. A structural basis for drug-induced long QT syndrome. Proc Natl Acad Sci U S A 2000;97:12329–33.
[52] Kamiya K, Niwa R, Mitcheson JS, Sanguinetti MC. Molecular determinants of HERG channel block. Mol Pharmacol 2006;69:1709–16.
[53] Perry M, Stansfeld PJ, Leaney J, Wood C, de Groot MJ, Leishman D, et al. Drug binding interactions in the inner cavity of HERG channels: molecular insights from structure–activity relationships of clofilium and ibutilide analogs. Mol Pharmacol 2006;69:509–19.
[54] Perry MD, deGroot MJ, Helliwell R, Leishman D, Sanguinetti MC. Structural determinants of HERG channel block by clofilium and ibutilide. Mol Pharmacol 2004;66:240–9.
[55] Chen J, Seebohm G, Sanguinetti MC. Position of aromatic residues in the S6 domain, not inactivation, dictates cisapride sensitivity of HERG and eag potassium channels. Proc Natl Acad Sci U S A 2002;99:12329–33.
[56] Splawski I, Shen J, Timothy KW, Lehmann MH, Priori S, Robinson JL, et al. Spectrum of mutations in long-QT syndrome genes. KvLQT1, HERG, SCN5A, KCNE1 and KCNE2. Circulation 2000;102:1175–85.
[57] Clarke CE, Hill AP, Zhao J, Kondo M, Subbiah RN, Campbell TJ, et al. Effect of S5P 7Q299. alpha-helix charge mutants on inactivation of hERG K^+ channels. J Physiol; 2006;573:730.291–304.
[58] Pless SA, Galpin JD, Frankel A, Ahern CA. Molecular basis for class Ib anti-arrhythmic inhibition of cardiac sodium channels. Nat Commun 2011;2:351. http://dx.doi.org/10.1038/ncomms1351.
[59] Hanck DA, Nikitina E, McNulty MM, Fozzard HA, Lipkind GM, Sheets MF. Using lidocaine and benzocaine to link sodium channel molecular conformations to state-dependent antiarrhythmic drug affinity. Circ Res 2009;105(5):492–9.
[60] Tikhonov DB, Bruhova I, Zhorov BS. Atomic determinants of state-dependent block of sodium channels by charged local anesthetics and benzocaine. FEBS Lett 2006;580:6027–32.
[61] Tan QY, Li HD, Zhu RH, Zhang QZ, Zhang J, Peng WX. Tolerability and pharmacokinetics of ranolazine following single and multiple sustained release doses in healthy Chinese adult volunteers: a randomized, open-label, Latin square design, phase I study. Am J Cardiovasc Drugs 2013;13:17–25.
[62] Lui HK, Harris FJ, Chan MC, Lee G, Mason DT. Comparison of intravenous mexiletine and lidocaine for the treatment of ventricular arrhythmias. Am Heart J 1986;112:1153–8.
[63] Silke B, Frais MA, Verma SP, Reynolds GW, Hafizullah M, Kalra PA, et al. Comparative haemodynamic effects of intravenous lignocaine, disopyramide and flecainide in uncomplicated myocardial infarction. Br J Clin Pharmacol 1986;22:707–14.
[64] Burashnikov A, Di Diego JM, Zygmunt AC, Belardinelli L, Antzelevitch C. Atrial-selective sodium channel block as a strategy for suppression of atrial fibrillation. Ann N Y Acad Sci 2008;1123:105–12.

[65] Vizzardi E, D'Aloia A, Quinzani F, Bonadei I, Rovetta R, Bontempi L, et al. A focus on antiarrhythmic properties of ranolazine. J Cardiovasc Pharmacol Ther 2012;17:353–6.
[66] Luderitz B, Mletzko R, Jung W, Manz M. Combination of antiarrhythmic drugs. J Cardiovasc Pharmacol 1991;17(Suppl. 6):S48–52.
[67] Opincariu M, Varro A, Iost N, Virag L, Hala O, Szolnoki, et al. The cellular electrophysiologic effect of a new amiodarone like antiarrhythmic drug GYKI 16638 in undiseased human ventricular muscle: comparison with sotalol and mexiletine. Curr Med Chem 2002;9:41–6.
[68] Matyus P, Varga I, Rettegi T, Simay A, Kallay N, Karolyhazy L, et al. Novel antiarrhythmic compounds with combined class IB and class III mode of action. Curr Med Chem 2004;11:61–9.
[69] Schimpf R, Wolpert C, Bianchi F, Giustetto C, Gaita F, Bauersfeld U, et al. Congenital short QT syndrome and implantable cardioverter defibrillator treatment: inherent risk for inappropriate shock delivery. J Cardiovasc Electrophysiol 2003;14:1273–7.
[70] Giustetto C, Schimpf R, Mazzanti A, Scrocco C, Maury P, Anttonen O, et al. Long-term follow-up of patients with short QT syndrome. J Am Coll Cardiol 2011;58:587–95.